Photoinduced enhancement of superconductivity in the plaquette Hubbard model

Yuxi Zhang [1], Rubem Mondaini [2], and Richard T. Scalettar[1]

[1]*Department of Physics, University of California, Davis, California 95616, USA*
[2]*Beijing Computational Science Research Center, Beijing 100084, China*

Real-time dynamics techniques have proven increasingly useful in theoretically and experimentally understanding strongly correlated systems. By employing unbiased time-resolved exact diagonalization, we study pump dynamics in the two-dimensional plaquette Hubbard model, where distinct hopping integrals t_h and t'_h are present within and between plaquettes. In the intermediate coupling regime, a significant enhancement of d-wave superconductivity is observed and compared with that obtained by simply examining expectation values with the eigenstates of the Hamiltonian. Our work provides a further understanding of superconductivity in the Hubbard model, extends the description of the pairing amplitude to the frequency-anisotropy plane, and offers a promising approach for experimentally engineering emergent out-of-equilibrium states.

I. INTRODUCTION

Out-of-equilibrium dynamics and photoinduced properties have been attracting intense attention recently. In a single-particle setting, periodic drives provide an additional "Floquet dimension" and can result in phenomena such as engineered Chern insulating behavior and Wannier-Stark localization [1]. These techniques have also allowed considerable new insight into strongly correlated systems and many-body phases induced by either electron-electron or electron-phonon interactions [2–5], including studies of photoinduced η pairing [6,7], bond-order wave (BOW) physics [8], dynamical topological engineering [9,10], and especially superconductivity [11–19], both theoretically and experimentally. A focus has been on gaining new insight into cuprate systems and the origin of pairing in high-T_c materials [20–23].

One mechanism for the enhancement of superconductivity is the use of photoexcitation to transfer charge between orbitals, thereby shifting the doping away from 1/8 filling where the "stripe anomaly" leads to a suppressed T_c. Here exact diagonalization studies have clarified whether the emergence of superconductivity via photoexcitation seen experimentally results from phonon or electronic mechanisms [16]. Indeed, superconductivity can also be developed out of the 1/8 filling phase through photoexcitation of the Cu-O stretch mode in the plane of the stripes [11]. This coupling to vibrational modes offers advantages in that the lower-energy photons are less likely to create high-temperature electronic distributions and heat the lattice.

In calculations similar to the study described here, a theoretical understanding of the enhancement of pairing is provided through lifting the degeneracy between superconducting and charge density wave (CDW) ground states in the attractive Hubbard Hamiltonian [14]. In the Hubbard-Holstein model, inducing d-wave pairing is especially effective at the quantum boundary between the CDW and spin density wave

(SDW) ground-state phases [16]. Theoretical work within a BCS model has also explored the role of the symmetry of the pair wave function. The existence of nodes in a d-wave phase allows for a more rapid decay, making the dynamics substantially faster than the s-wave channel [12].

In parallel with these developments, theoretical studies have shown that inhomogeneities such as stripelike or plaquette decorations of two-dimensional square lattices could enhance d-wave pairing in equilibrium [24–34]. This is an especially rich area of inquiry given the complex entwining of spin and charge textures with pairing [35–40]. Specifically, inhomogeneities clearly interfere with superconductivity under some circumstances, while in others, they appear to play a role in its formation and stability.

In this paper, we *combine* these two themes of out-of-equilibrium dynamics and spatial inhomogeneity. In particular, we examine the effect of pumping on a geometry built up from attractive d-wave binding centers formed by 2×2 plaquettes. Our goal is to understand the interplay of these two effects, which are already known *individually* to result in enhanced superconductivity. Our work will therefore examine the possibility that a greater signal of pairing might be thereby engineered, a prospect made particularly intriguing by the recent experimental emulation of fermionic models in 2×2 plaquettes in platforms of quantum dots [41].

The next section introduces the plaquette Hubbard model and our computational methodology. We then examine the degree of d-wave pairing in the different low-energy eigenstates. A central result here is a "phase diagram" which shows the degree of enhanced superconductivity in the plane of hopping anisotropy t'_h/t_h and excitation energy $E_\alpha - E_0$. We next examine time evolution, with the objective of employing a quasiperiodic drive of an appropriate frequency ω_0 to target those optimal $E_\alpha - E_0$. The end result is a second "phase diagram," which indicates the achievable enhancement in the plane of ω_0 and drive amplitude A_0. Here we focus on the t'_h/t_h,
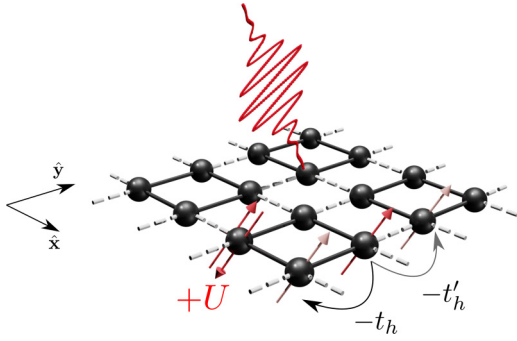
FIG. 1. Schematic illustration of the plaquette Hubbard model on a 4×4 lattice with PBCs, with relevant terms in the Hamiltonian annotated. Dark-colored (light-colored) bonds represent the intraplaquette (interplaquette) hopping t_h (t'_h).

which gives optimal pairing in the analysis of the eigenstates. We conclude the paper with a summary of the results and a discussion of the general significance of our findings.

II. MODEL AND METHODOLOGY

The two-dimensional Hubbard model is described by

$$\hat{\mathcal{H}} = -\sum_{\langle \mathbf{i},\mathbf{j}\rangle,\sigma} (t_{\mathbf{i},\mathbf{j}}\, \hat{c}_{\mathbf{i}\sigma}^{\dagger}\hat{c}_{\mathbf{j}\sigma} + \text{H.c.}) + U\sum_{\mathbf{i}}\hat{n}_{\mathbf{i},\uparrow}\hat{n}_{\mathbf{i},\downarrow}, \quad (1)$$

where $\hat{c}_{\mathbf{i}\sigma}$ ($\hat{c}_{\mathbf{i}\sigma}^{\dagger}$) is the annihilation (creation) operator for an electron on-site $\mathbf{i}$ with spin $\sigma = \uparrow,\downarrow$ and $\hat{n}_{\mathbf{i},\sigma} = \hat{c}_{\mathbf{i},\sigma}^{\dagger}\hat{c}_{\mathbf{i},\sigma}$ is the number operator. $t_{\mathbf{i},\mathbf{j}} = t_h$ (t'_h) gives the hopping integral within (between) plaquettes, and on-site electron-electron interaction is tuned via U. We set $t_h = 1$ as the energy scale, and the time t is measured in terms of t_h^{-1} with $\hbar = 1$. Throughout this paper, we use an $N = 4\times4$ lattice with periodic boundary conditions (PBCs), as illustrated in Fig. 1. The system is driven by a time-dependent external field, which is introduced in the Hamiltonian via the Peierls substitution

$$t_{\mathbf{i},\mathbf{j}}\, \hat{c}_{\mathbf{i}\sigma}^{\dagger}\hat{c}_{\mathbf{j}\sigma} + \text{H.c.} \rightarrow t_{\mathbf{i},\mathbf{j}}\, e^{i\mathbf{A}(t)\cdot(\mathbf{r}_{\mathbf{i}}-\mathbf{r}_{\mathbf{j}})}\, \hat{c}_{\mathbf{i}\sigma}^{\dagger}\hat{c}_{\mathbf{j}\sigma} + \text{H.c.}, \quad (2)$$

where $\mathbf{A}(t)$ is the spatially uniform vector potential. We choose $\mathbf{A}(t)$, mimicking an ultrafast photoirradiation, of the form

$$\mathbf{A}(t) = A_0 e^{-(t-t_0)^2/2t_d^2}\, \cos[\omega_0(t-t_0) + \varphi]\, \mathbf{e}_{\text{pol}}, \quad (3)$$

i.e., an oscillatory Gaussian centered at t_0 and width t_d, with amplitude A_0, frequency ω_0, and polarization direction $\mathbf{e}_{\text{pol}} = (\hat{\mathbf{x}} + \hat{\mathbf{y}})/\sqrt{2}$. Finally, φ is a time phase of the pump pulse, allowing the possibility of phase averaging that eliminates particular fast coherent oscillations tied to interaction magnitudes [2]. When applicable, results of the dynamics will employ an average over ten equidistant values of φ in the range $[0, 2\pi)$. In what follows, we set $t_0 = 100\, t_h^{-1}$ and $t_d = 25\, t_h^{-1}$, with maximum time chosen as $t_{\text{max}} = 200\, t_h^{-1}$, which is well after the pump still exhibits a relevant amplitude.

Simulations are carried out with the time-dependent Lanczos method [42,43], where the time evolution is obtained via $|\Psi(t + dt)\rangle = e^{-i\hat{\mathcal{H}}(t)dt}|\Psi(t)\rangle$, with dt being a sufficiently small time step. The initial state, $|\Psi(t \to -\infty)\rangle$, is the ground state of (1), with $|\Psi(t)\rangle$ and associated measurements being evaluated at each time step.

III. EQUILIBRIUM RESULTS

To map out where an out-of-equilibrium protocol would induce enhanced superconductivity, we start by examining the equilibrium properties of the plaquette Hubbard model across a range of $(t'_h/t_h, U, n_e)$ parameters. Some of these have already been explored at finite temperatures utilizing quantum Monte Carlo simulations [31] or at the ground state [26] in lattice sizes as in Fig. 1. Reexamination of ground-state properties is included in Appendix A. Here, we go beyond that and investigate different equal-time correlators computed over the low-lying eigenspectrum of (1) $[\hat{\mathcal{H}}|\alpha\rangle = E_\alpha|\alpha\rangle]$. Among them, we calculate the pairing structure factor at different γ channels

$$P_\gamma = \frac{1}{N}\sum_{\mathbf{i},\mathbf{dr}} \langle \hat{\Delta}_{\mathbf{i}}^{(\gamma)}\, \hat{\Delta}_{\mathbf{i}+\mathbf{dr}}^{(\gamma)\dagger}\rangle, \quad (4)$$

where $\hat{\Delta}_{\mathbf{i}}^{(\gamma)} = (\hat{c}_{\mathbf{i}+\hat{\mathbf{x}},\sigma} + f(\gamma)\hat{c}_{\mathbf{i}+\hat{\mathbf{y}},\sigma})\hat{c}_{\mathbf{i},\overline{\sigma}}$, with $f(\gamma) = -1$ (+1) for d-wave (extended s-wave, s^*) pairing. In a similar fashion, the *staggered* spin and charge correlations are probed as

$$S_x = \frac{1}{N}\sum_{\mathbf{i},\mathbf{dr}} \langle(-1)^{dx+dy}\hat{O}_{\mathbf{i}}^{\dagger}\hat{O}_{\mathbf{i}+\mathbf{dr}}\rangle, \quad (5)$$

where $\hat{O}_{\mathbf{i}} = \hat{n}_{\mathbf{i}\uparrow} \pm \hat{n}_{\mathbf{i}\downarrow}$, where the "+" sign defines charge ($x = $ CDW) and the "−" sign spin ($x = $ SDW) density wave order. Structure factors are useful to probe long-range order; however, given the lattice size available, the differentiation from short-range (local) order is difficult. We use structure factors since they provide a more global measure of correlations across the lattice. Local correlators, including double occupancies in the homogeneous setting ($t_h = t'_h$), have been previously studied [44].

Over the large set of parameters available, we focus the investigation on both the doped ($\rho \equiv n_e/N = 0.875$) and undoped cases ($\rho = 1$); the latter is described in Appendix B. Due to geometric constraints in the lattice size we tackle, a period-8 magnetic stripe formation is not supported [38,45–47]. The ground-state properties of $\hat{\mathcal{H}}$, originally reported in Ref. [26], indicated that maximum binding energy at small hole dopings occurs at intermediate plaquette hopping energies ($t'_h/t_h \simeq 0.5$) and large repulsive interactions $U \simeq 8\, t_h$. This serves as a paradigm for our investigation, in which we are interested in the set of parameters that maximize the expectation values of pairing correlators over states beyond that of the ground state $|0\rangle$. Figure 2 displays the eigenstate expectation values (EEVs) of the previously introduced correlators for $t'_h/t_h = 0.8$, $U = 8\, t_h$. Most noticeably, a group of three excited states (two of them degenerate) with energy gap $E_\alpha - E_0 \simeq 0.25\, t_h$ (belonging to the same momentum sector) has d-wave pairing $P_d \simeq 1.9$, significantly higher than that of the ground state $P_d = 1.66$. With the exception of the staggered spin correlations, no similar substantial relative increase is seen in other correlators, including the extended s-wave or CDW channels. Equivalent simulations were performed for
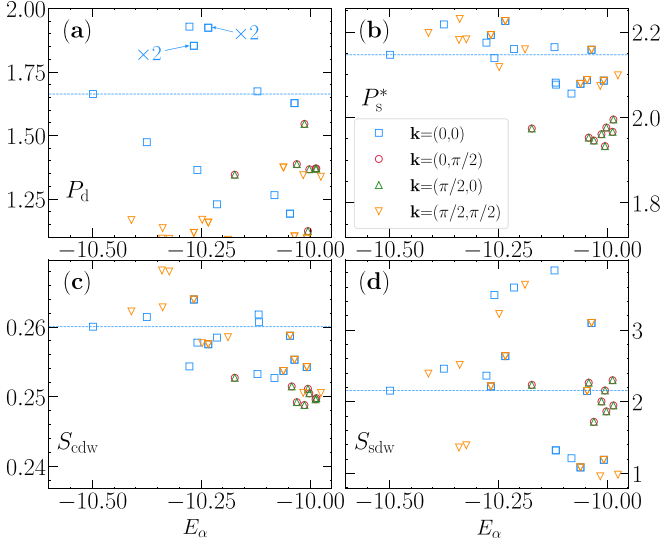
FIG. 2. (a) d-wave, (b) extended s-wave, (c) CDW, and (d) SDW structure factor, in the ground state (dashed lines) and the first few excited states. Different colors and symbols represent different quasi-momentum sectors. Parameters used are $t'_h/t_h = 0.8$, $U = 8\,t_h$, and $n_e = 14$. We show the different momentum sectors $\mathbf{k}$ for completeness since, for this filling, the ground state always resides at $\mathbf{k} = (0, 0)$. Each sector displays various eigenstates $|\alpha\rangle$, some of which may display degeneracies owing to other point group symmetries not being resolved, e.g., mirror symmetries.

other t'_h/t_h values, and a compilation of the results of the relative maximum enhancement over excited states with respect to the ground state, $\Delta\mathcal{O} \equiv (\max\{\langle\alpha|\hat{\mathcal{O}}|\alpha\rangle\} - \langle 0|\hat{\mathcal{O}}|0\rangle)/\langle 0|\hat{\mathcal{O}}|0\rangle$, is given in Fig. 3. Although this maximum increase for the d-wave pairing is seen right in the vicinity of the homogeneous system ($t'_h = t_h$), we focus on $t'_h/t_h = 0.8$ to study the regime of robustly formed plaquettes.
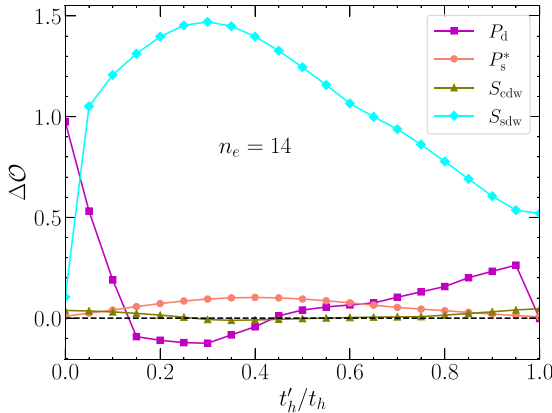

FIG. 3. Relative variation of the maximum eigenstate expectation values $\Delta\mathcal{O}$, quantified over excited states, with respect to its ground-state average (see text) for different correlators, when taking into account at least 24 eigenstates in the low-lying spectrum for the $\mathbf{k} = (0, 0)$ momentum sector. Parameters are the same as in Fig. 2: $U = 8\,t_h$ and $n_e = 14$. Notice that an anticorrelation between spin and d-wave pairing enhancement can be seen as t'_h/t'_h is increased.
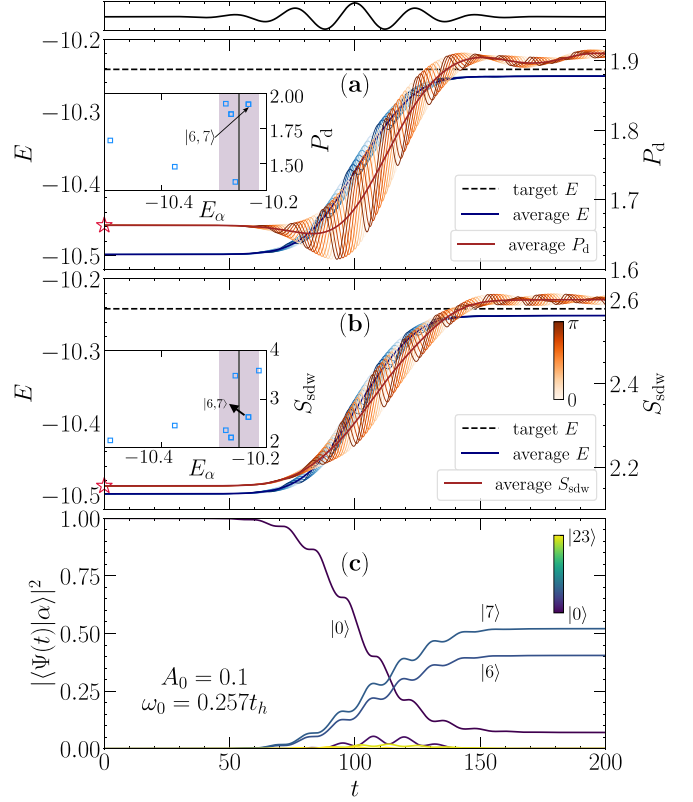

FIG. 4. Top panel: schematics of the pulse amplitude over time. (a) Evolution of the phase-averaged d-wave pair correlation P_d (red solid curve) and mean energy E (blue solid curve). The different curves in shades of red and blue denote the values for each time phase φ. (b) The same for the staggered spin structure factor. (c) Dynamics of the overlaps $|\langle\Psi(t)|\alpha\rangle|^2$ over the course of photoirradiation. Darker-colored curves represent lower-energy states; the degenerate doublet, $|6\rangle$ and $7\rangle$, displays the largest contribution to $|\Psi(t)\rangle$ as marked, whereas the participation of $|0\rangle$, the initial state, diminishes significantly. The insets in (a) and (b) give the EEVs for both quantities with the mean energy at $t = t_{\max}$ and within a window given by σ_E (see text); EEVs in the degenerate eigenstates $|6, 7\rangle$ are also marked. Pump parameters are $A_0 = 0.1$ and $\omega_0 = 0.257\,t_h$.

IV. OUT-OF-EQUILIBRIUM RESULTS: PHOTOIRRADIATION

Having established that the expectation values of correlators, in particular P_d, measured in excited eigenstates of the Hamiltonian may possess larger values in comparison to the ones at the ground state, we turn to the out-of-equilibrium scenario, with an added time-dependent external field which can cause transitions to these states. Its associated vector potential amplitude is depicted at the top of Fig. 4. We follow a procedure that has been proven feasible in other contexts of photoirradiation [8,10]: By using a fine-tuned temporal perturbation, whose frequency is set resonantly with the target state one is aiming to excite ($\omega_0 \equiv E_{\mathrm{target}} - E_0$), the dynamics at long times thus exhibit a large overlap with such an eigenstate.

There are a number of constraints in this protocol. First, the initial and final states need similar quantum numbers: in particular, total momentum, as the vector potential used [Eq. (3)]

is spatially uniform and does not break translation invariance. Second, the pump needs to be time constrained; otherwise the system would indefinitely absorb energy from the drive, owing to the thermalizing properties of nonintegrable systems [48]. In such a case, heating towards an infinite-temperature regime would ensue at sufficiently long times, exhibiting featureless correlators.

Following these requirements, we use a pump with parameters $A_0 = 0.1$, $\omega_0 = 0.257 t_h$ to closely match that of the excited states with stronger d-wave pairing signal [see the top of Fig. 2(a)]. These parameters are also reasonably aligned with the ones employed in recent experiments. Using $t_h \simeq 0.3$ eV, which is typically seen in most cuprate materials, $\omega_0 = 0.257 t_h$ corresponds to 0.08 eV or 20 THz whereas $A_0 = 0.1$ translates into a pump fluence of ~ 0.02 J/cm^2; these values are comparable to those used in photoinduced experiments [11,23]. A discussion of the neighboring frequencies that can influence the dynamics and the reason why we chose this specific ω_0 is given in Appendix C. One can, however, see from Fig. 2 that this ω_0 at least roughly corresponds to the excitation energy of a set of states with enhanced P_d. In particular, a doublet of states ($|6\rangle$ and $|7\rangle$), energy degenerate up to $10^{-12} t_h$, possesses one of the largest expectation values of the d-wave pairing P_d ($\simeq 1.92$). Under these conditions, Fig. 4(a) shows that a considerable enhancement in d-wave pairing is induced, accompanied by an energy increase, such that the mean energy at long times, $E = \langle \Psi(t = t_{\max})|\hat{\mathcal{H}}|\Psi(t = t_{\max})\rangle$, is close to the eigenenergy of the target states. Simultaneously, a similar large enhancement on the staggered spin correlations is also achieved [Fig. 4(b)].

To demonstrate that the dynamics is being influenced by the target and its neighboring states at these time scales, we compute the overlaps of the time-evolving wave functions and the eigenstates of the equilibrium Hamiltonian, $|\langle \Psi(t)|\alpha \rangle|^2$. We report those in Fig. 4(c), where one notices that the weight of the target doublet states rises up to 0.52 and 0.40 after the pump, for states $|7\rangle$ and $|6\rangle$, respectively, explaining thus the enhancement of d-wave pairing under these conditions. The participation of the ground state $|0\rangle$ decreases significantly, whereas the contribution of other eigenstates is mostly negligible. In the insets of Figs. 4(a) and 4(b), the EEVs of P_d and S_{sdw} are shown in this set of parameters, $(U/t_h, t'_h/t_h) = (8, 0.8)$, together with the mean energy of the system $E(t_{\max})$.

A first account of which eigenstates can significantly contribute to the dynamics at a given time is given by the width in energy of $|\Psi(t)\rangle$, defined as $\sigma_E = [\langle \Psi(t)|H^2|\Psi(t)\rangle - \langle \Psi(t)|H|\Psi(t)\rangle^2]^{1/2}$ [49,50]. This is displayed as a shaded area surrounding $E(t_{\max})$ in the insets of Figs. 4(a) and 4(b), where we notice that the eigenstates within the window are the ones that may display a large overlap with $|\Psi(t)\rangle$ in Fig. 4(c). While this window contains six eigenstates in the $\mathbf{k} = (0, 0)$ quasimomentum sector, not all of them affect the dynamics. Symmetry requirements related to how they couple to the current operator $\hat{\mathcal{J}} = \sum_{\langle \mathbf{i}, \mathbf{j} \rangle, \sigma} (-it_{\mathbf{i}, \mathbf{j}} \hat{c}^\dagger_{\mathbf{i}\sigma} \hat{c}_{\mathbf{j}\sigma} + \mathrm{H.c.})$ dictate which ones will eventually couple to the external field. That is, besides energy requirements, overlaps $|\langle \alpha|\hat{\mathcal{J}}|0\rangle|^2$ also classify, in first order, the states most influencing the dynamics. Even if the pulse maintains the quasimomentum of the time-evolving wave function, the polarization employed is insufficient to mix all different mirror symmetry sectors. As a
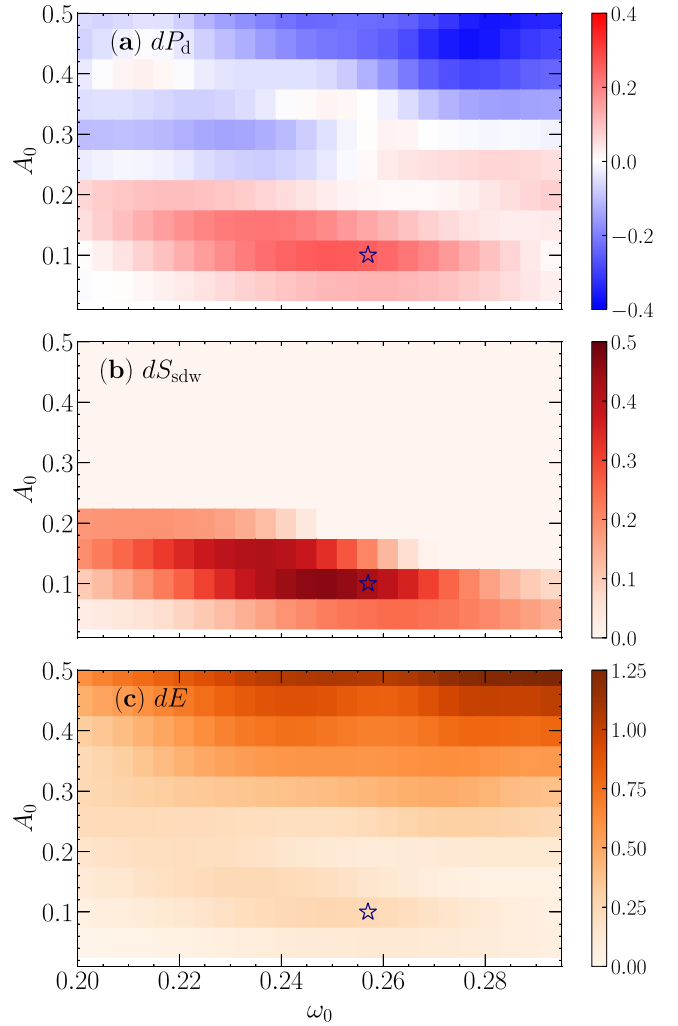

FIG. 5. Contour plots of the enhancement of the d-wave pair structure factor (a) and staggered spin structure factor (b) at $t = t_{\max}$ for various pump parameter (A_0, ω_0) values. (c) Similar results for the injected energy by the photoirradiation. All results are obtained for $\varphi = 0$. In all panels, star markers identify the pump parameters used in Fig. 4.

result, some eigenstates must not participate in the dynamical evolution process.

Now that we have confirmed that an enhancement of d-wave pairing is attainable for these pump parameters, we explore other combinations of (A_0, ω_0), identifying the ones that give optimal results in the enhancement of pair correlations at long times. Towards that end, we study the variation of different post-pump observables as $dP_d \equiv P_d(t = t_{\max}) - P_d(0)$ [Fig. 5(a)] and $dS_{\mathrm{sdw}} \equiv S_{\mathrm{sdw}}(t = t_{\max}) - S_{\mathrm{sdw}}(0)$ [Fig. 5(b)], quantifying the dynamical variations of d-wave pairing and staggered spin correlations. A relatively narrow band in pump amplitudes A_0 increases pairing for resonant drives. The reason can be seen by the map of injected energies $dE \equiv E(t = t_{\max}) - E_0$ in Fig. 5(c): Increasing A_0 leads to a systematically larger absorbed energy by the system; thereby a larger contribution of states in the bulk of the spectrum, not associated with an enhanced pairing amplitude, is manifest.

We note that not only is a specific resonant drive with frequency ω_0, in principle, able to target a state, but also higher harmonic contributions $2\omega_0$, $3\omega_0$, … are able to target a state. A tuning of other parameters of the pulse, as A_0 and t_d, is necessary for these conditions to control the injected energy in the system while monitoring the typical width in energy of $|\Psi(t_{\max})\rangle$. Adjusting these parameters within physically reasonable limits thus presents as a systematic protocol to access the physics of competing states close to the ground state, guaranteeing that the long-time dynamics is largely influenced by the (group of) target excited state(s). Such entwining of different correlations is known to occur in doped Hubbard Hamiltonians, and, as we demonstrated, engineered time-dependent perturbations are key to picking one (or more) type in detriment of others.

V. SUMMARY AND DISCUSSION

We studied the plaquette Hubbard model under photoirradiation, with a goal of dynamical enhancement of d-wave superconductivity. By focusing on a regime away from half filling ($\rho = 0.875$), we observed a moderate increase of pairing (15% for $t'_h/t_h = 0.8$) at long times in relation to the equilibrium ground state. Enhanced staggered spin fluctuations accompany this. Such correlated behavior is not unfamiliar to the physics of unconventional superconductors, where a close competition or entwining of states displaying spin and pairing order is known to occur. That we dynamically reach a simultaneous enhancement of both pair and spin degrees of freedom provides a further, interesting window into the interplay of the low-energy physics of the weakly doped Hubbard model.

A fundamental difference between our study and others that have numerically investigated the increase of superconducting correlations in time is that, in our case, the unperturbed Hamiltonian does not feature strong charge or spin fluctuations associated with long-range order. In particular, the unperturbed system is not a Mott insulator as in Ref. [6] or a Peierls insulator as in Ref. [16]. Consequently, the gaps separating the ground state and other excited states are substantially smaller. This is one reason why our pump pulses have approximately one order of magnitude smaller frequencies.

On the other hand, our protocol is intrinsically tied to the specific details of the Hamiltonian's low-lying spectrum and can be used more generally to induce changes in the wave-function characteristics, surpassing the specific focus on superconductivity [8,10]. It is worth noticing that a requirement to achieve an efficient targeting of states is that these are well separated in energy from the bulk of the spectrum. Otherwise, the overlaps with nondesired states are unavoidable. When approaching the thermodynamical limit (not addressed here), the low-lying eigenspectrum is still discrete (that is, it does not form a continuous bulk), and identification of a targeting protocol is still feasible.

Nonetheless, confirming these results in larger cluster sizes may shed light on the understanding of its impact in explaining potential connections to experimental results. We stress, however, that in dealing with small clusters, finite-size effects for d-wave correlators do not monotonically decrease with the system size but are rather influenced by the number z_d of independent neighboring d-wave plaquettes [51]. In the thermodynamic limit $z_d = 4$, the smallest cluster size featuring such a configuration possesses $N = 20$ (the 4×4 cluster has $z_d = 2$). This sits on the verge of what is computationally accessible within the scope of exact numerical methods. While the excitation energy to states with higher P_d certainly depends on the cluster size, an appropriate change in the pulse frequency can handle the correct targeting scheme. What is less obvious is whether such excited states exist as the cluster size grows. It is likely they do since the typical correlation length for d-wave pairing is short. However, a systematic study for larger system sizes is left for future studies.

A potential avenue of future investigation is to understand the competition of charge textures (as stripes) and pairing, now adding real-time dynamics to potentially enhance one degree of freedom in detriment of the other. This builds prospects to connect to recent experimental results in cuprates [20,22,23,52]. A word of caution, however, is that realistic treatment of such materials using model Hamiltonians might necessarily take into account either phonon degrees of freedom [18] or the effects of multiple bands [53], such as the distinct Cu and O orbitals. Still, the "bottom-up" approach we develop to first understand the physics of the low-lying spectrum to justify dynamical modifications of suitable correlators should similarly work.

APPENDIX A: GROUND-STATE PROPERTIES

In the main text, the focus is on the dynamic enhancement of certain correlations based on the properties of the low-lying spectrum. Here we present a few extra details about the ground state, i.e., properties of the initial states before the photoirradiation. The pair-binding energy and (selected) pair correlations on the ground state of the Hamiltonian (1) were originally characterized in Ref. [26] in the same lattice size and over different hole dopings. We now present additional metrics in Fig. 6 for $\rho = 0.875$ and $U/t_h = 8$. To start, we quantify the nearest-neighbor density [Fig. 6(a)] and spin [Fig. 6(b)] correlations as a function of the interplaquette hopping t'_h.

By resolving the correlations within and connecting plaquettes (that is, on the t_h and t'_h bonds), we show that the density correlations $C^{x=n}_{\langle \mathbf{ij} \rangle} \equiv \langle \hat{O}_{\mathbf{i}} \hat{O}_{\mathbf{j}} \rangle - \langle \hat{O}_{\mathbf{i}} \rangle \langle \hat{O}_{\mathbf{j}} \rangle$, where $\hat{O}_{\mathbf{i}} = \hat{n}_{\mathbf{i}\uparrow} + \hat{n}_{\mathbf{i}\downarrow}$, exhibit a clear trend of evolution when plaquettes are increasingly "connected," resulting in stronger interplaquette correlations at the expense of slightly reduced ones within a plaquette. For spin degrees of freedom, $C^{x=m}_{\langle \mathbf{ij} \rangle}$ with $\hat{O}_{\mathbf{i}} = \hat{n}_{\mathbf{i}\uparrow} - \hat{n}_{\mathbf{i}\downarrow}$, the t_h-mediated correlations denote an
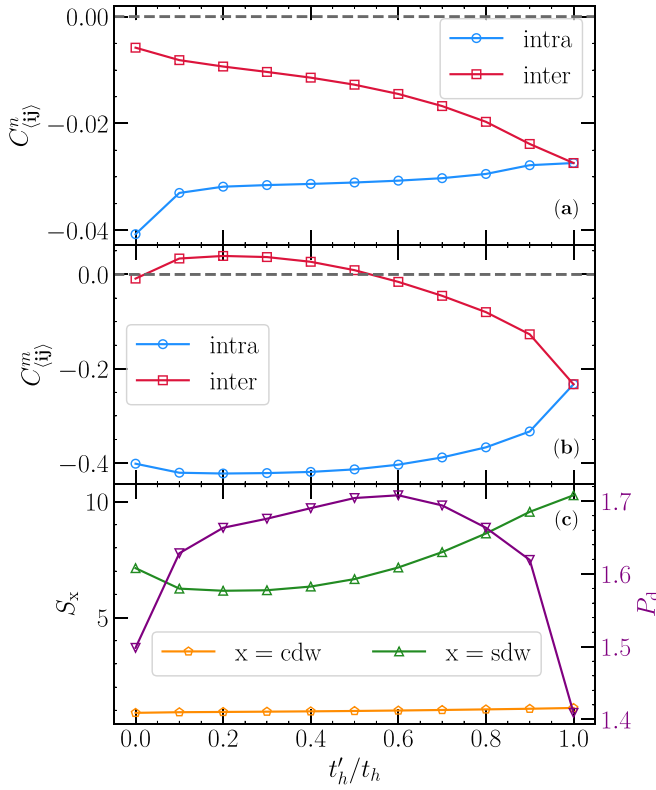
FIG. 6. Nearest-neighbor density (a) and spin correlations (b) as a function of the hopping connecting plaquettes. These are resolved by whether the nearest neighbor belongs to the same plaquette ("intra") or to a neighboring one ("inter"). (c) The dependence of the structure factors defined in the main text on t'_h; the right axis gives the scale for P_d. The parameters are $U/t_h = 8$ and $\rho = 0.875$. Notice that the values at $t'_h = 0$ can result in the contribution of a mix of occupancies since this density is not commensurate with a four-site isolated plaquette.

intraplaquette antiferromagnetic ordering throughout the range $t'_h \in [0, t_h]$ studied, but global short-ranged antiferromagnetic ordering is only obtained when $t'_h \gtrsim 0.5t_h$; this is the regime we focus on in the main text concerning photoirradiation.

Quantum Monte Carlo results at low-but-finite temperatures, in lattices with twice as large linear size [31], indicate that this ferromagnetic interplaquette ordering is not manifested: It is thus likely an indication of finite-size effects that we can avoid by selecting a larger t'_h. Lastly, Fig. 6(c) gives the dependence of the previously described structure factors: S_{cdw} is largely constant, while S_{sdw} steadily increases with t'_h. The d-wave pair structure factor exhibits optimal values at intermediate interplaquette couplings, similar to the results of Ref. [26] obtained for a single pair-pair correlator. Notably, P_d has a maximum when the interplaquette spin correlations turn antiferromagnetic, another piece of evidence of the entwining of different orders in the model.

APPENDIX B: THE HALF-FILLED CASE

In the main text, we focus on the case of a hole-doped system ($n_e = 14$), guided by the enhanced superconducting properties in cuprate materials in these conditions and by the
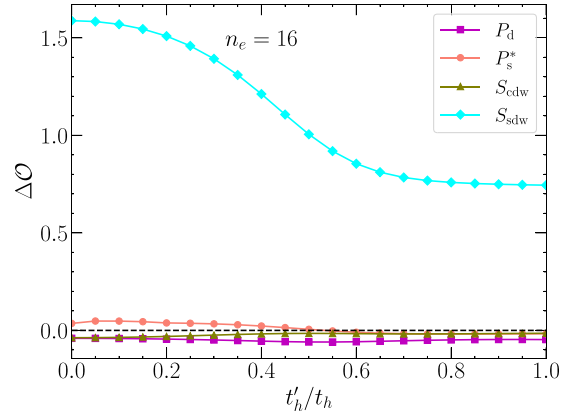

FIG. 7. The equivalent of Fig. 3, but for the half-filled system at $U/t_h = 8$. Within a span of 24 eigenstates of the low-lying spectrum at zero quasimomentum (the same where the ground state resides), no significant increase of matrix elements for pairing correlators with respect to its ground-state average is observed.

large pair-binding energy observed in a similar Hamiltonian [26]. Yet, the possibility that enhanced pairing can be obtained even when the parent system is a robust insulator has also been proven before [6,16]. Thus, using our guiding protocol to infer the likelihood of a photoirradiation perturbation, assessing first the properties of the low-lying spectrum, in Fig. 7 we compute the largest relative enhancement of correlators at half filling ($n_e = 16$), in analogy to Fig. 3.

We notice that other than potentially larger spin fluctuations, the remaining observables we investigate do not possess large matrix elements in the low-lying eigenspectrum compared with the ground state. As a result, no significant dynamical enhancement of pairing is expected in this scenario, including, specifically, d-wave pairing.

APPENDIX C: ENHANCEMENT OF d-WAVE PAIRING AT NEIGHBORING FREQUENCIES

In the main text, we have used a specific pump frequency, $\omega_0 = 0.257 t_h$. Here we discuss the rationale behind this
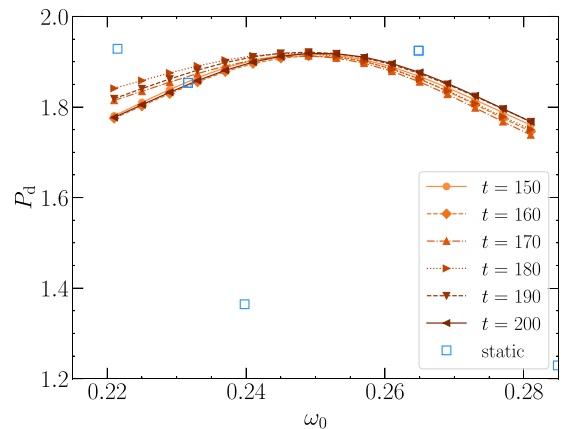

FIG. 8. The phase-averaged value of the d-wave pairing correlator at various late times as marked. Open squares give the expectation values within various low-lying eigenstates.

choice, based on the results for the phase-averaged enhancement of the P_d pairing correlators at different long times, as displayed in Fig. 8. The maximum enhancement of the d-wave pairing at times following the pulse is obtained for frequencies ω_0 slightly below $E_{6,7} - E_0 = 0.2648 t_h$. The reason is that, despite the target doublet states being mostly excited, contributions from other states to the dynamics, as, e.g., state $|1\rangle$, lead to an optimal selection of pump parameters that are slightly below a simple locked-in frequency analysis at $E_{\text{target}} - E_0$. Tuning to a slightly smaller $\omega_0 = 0.257 t_h$ lessens the excitation amplitude to the biggest P_d states, but that is

more than compensated by a similar lessening of the excitation amplitude to the two states with smaller P_d.

In other contexts, when initial and target states are related by a first-order phase transition in a slightly different regime of parameters of the Hamiltonian, resonant selection of the states is often highly effective [8,10], since in such cases they are well separated from the bulk of the spectrum [54]. This may explain recent observations of enhancement of d-wave pairing in the vicinity of a phase boundary in systems where the interplay of electron and phonon degrees of freedom is present [16,18].

[1] T. Oka and S. Kitamura, Floquet engineering of quantum materials, Annu. Rev. Condens. Matter Phys. **10**, 387 (2019).

[2] Y. Wang, M. Claassen, B. Moritz, and T. Devereaux, Producing coherent excitations in pumped Mott antiferromagnetic insulators, Phys. Rev. B **96**, 235142 (2017).

[3] Y. Wang, M. Claassen, C. D. Pemmaraju, C. Jia, B. Moritz, and T. P. Devereaux, Theoretical understanding of photon spectroscopies in correlated materials in and out of equilibrium, Nat. Rev. Mater. **3**, 312 (2018).

[4] J. Tindall, F. Schlawin, M. Buzzi, D. Nicoletti, J. Coulthard, H. Gao, A. Cavalleri, M. Sentef, and D. Jaksch, Dynamical Order and Superconductivity in a Frustrated Many-Body System, Phys. Rev. Lett. **125**, 137001 (2020).

[5] J. Sous, B. Kloss, D. M. Kennes, D. R. Reichman, and A. J. Millis, Phonon-induced disorder in dynamics of optically pumped metals from nonlinear electron-phonon coupling, Nat. Commun. **12**, 5803 (2021).

[6] T. Kaneko, T. Shirakawa, S. Sorella, and S. Yunoki, Photoinduced η Pairing in the Hubbard Model, Phys. Rev. Lett. **122**, 077002 (2019).

[7] T. Shirakawa, S. Miyakoshi, and S. Yunoki, Photoinduced η pairing in the Kondo lattice model, Phys. Rev. B **101**, 174307 (2020).

[8] C. Shao, H. Lu, H.-G. Luo, and R. Mondaini, Photoinduced enhancement of bond order in the one-dimensional extended Hubbard model, Phys. Rev. B **100**, 041114(R) (2019).

[9] J. McIver, B. Schulte, F.-U. Stein, T. Matsuyama, G. Jotzu, G. Meier, and A. Cavalleri, Light-induced anomalous Hall effect in graphene, Nat. Phys. **16**, 38 (2020).

[10] C. Shao, P. D. Sacramento, and R. Mondaini, Photoinduced anomalous Hall effect in the interacting Haldane model: Targeting topological states with pump pulses, Phys. Rev. B **104**, 125129 (2021).

[11] A. Cavalleri, Photo-induced superconductivity, Contemp. Phys. **59**, 31 (2018).

[12] F. Peronaci, M. Schiró, and M. Capone, Transient Dynamics of d-Wave Superconductors after a Sudden Excitation, Phys. Rev. Lett. **115**, 257001 (2015).

[13] Y. Wang, B. Moritz, C.-C. Chen, C. Jia, M. van Veenendaal, and T. P. Devereaux, Using Nonequilibrium Dynamics to Probe Competing Orders in a Mott-Peierls System, Phys. Rev. Lett. **116**, 086401 (2016).

[14] M. A. Sentef, A. Tokuno, A. Georges, and C. Kollath, Theory of Laser-Controlled Competing Superconducting and Charge Orders, Phys. Rev. Lett. **118**, 087002 (2017).

[15] G. Mazza and A. Georges, Nonequilibrium superconductivity in driven alkali-doped fullerides, Phys. Rev. B **96**, 064515 (2017).

[16] Y. Wang, C.-C. Chen, B. Moritz, and T. P. Devereaux, Light-Enhanced Spin Fluctuations and d-Wave Superconductivity at a Phase Boundary, Phys. Rev. Lett. **120**, 246402 (2018).

[17] M. Buzzi, D. Nicoletti, M. Fechner, N. Tancogne-Dejean, M. A. Sentef, A. Georges, T. Biesner, E. Uykur, M. Dressel, A. Henderson, T. Siegrist, J. A. Schlueter, K. Miyagawa, K. Kanoda, M. S. Nam, A. Ardavan, J. Coulthard, J. Tindall, F. Schlawin, D. Jaksch *et al.*, Photomolecular High-Temperature Superconductivity, Phys. Rev. X **10**, 031028 (2020).

[18] Y. Wang, T. Shi, and C.-C. Chen, Fluctuating Nature of Light-Enhanced d-Wave Superconductivity: A Time-Dependent Variational Non-Gaussian Exact Diagonalization Study, Phys. Rev. X **11**, 041028 (2021).

[19] T. Tang, Y. Wang, B. Moritz, and T. P. Devereaux, Orbitally selective resonant photodoping to enhance superconductivity, Phys. Rev. B **104**, 174516 (2021).

[20] D. Fausti, R. Tobey, N. Dean, S. Kaiser, A. Dienst, M. C. Hoffmann, S. Pyon, T. Takayama, H. Takagi, and A. Cavalleri, Light-induced superconductivity in a stripe-ordered cuprate, Science **331**, 189 (2011).

[21] S. Kaiser, C. R. Hunt, D. Nicoletti, W. Hu, I. Gierz, H. Y. Liu, M. Le Tacon, T. Loew, D. Haug, B. Keimer, and A. Cavalleri, Optically induced coherent transport far above T_c in underdoped $YBa_2C_3O_{6+\delta}$, Phys. Rev. B **89**, 184516 (2014).

[22] D. Nicoletti, E. Casandruc, Y. Laplace, V. Khanna, C. R. Hunt, S. Kaiser, S. Dhesi, G. Gu, J. Hill, and A. Cavalleri, Optically induced superconductivity in striped $La_{2-x}Ba_xCuO_4$ by polarization-selective excitation in the near infrared, Phys. Rev. B **90**, 100503(R) (2014).

[23] K. A. Cremin, J. Zhang, C. C. Homes, G. D. Gu, Z. Sun, M. M. Fogler, A. J. Millis, D. N. Basov, and R. D. Averitt, Photoenhanced metastable c-axis electrodynamics in stripe-ordered cuprate $La_{1.885}Ba_{0.115}CuO_4$, Proc. Natl. Acad. Sci. USA **116**, 19875 (2019).

[24] W.-F. Tsai and S. A. Kivelson, Superconductivity in inhomogeneous Hubbard models, Phys. Rev. B **73**, 214510 (2006).

[25] H. Yao, W.-F. Tsai, and S. A. Kivelson, Myriad phases of the checkerboard Hubbard model, Phys. Rev. B **76**, 161104(R) (2007).

[26] W.-F. Tsai, H. Yao, A. Läuchli, and S. A. Kivelson, Optimal inhomogeneity for superconductivity: Finite-size studies, Phys. Rev. B **77**, 214502 (2008).

[27] D. G. S. P. Doluweera, A. Macridin, T. A. Maier, M. Jarrell, and T. Pruschke, Suppression of d-wave superconductivity in the checkerboard Hubbard model, Phys. Rev. B **78**, 020504(R) (2008).

[28] H. Yao and S. A. Kivelson, Fragile Mott Insulators, Phys. Rev. Lett. **105**, 166402 (2010).

[29] S. Baruch and D. Orgad, Contractor-renormalization study of Hubbard plaquette clusters, Phys. Rev. B **82**, 134537 (2010).

[30] P. M. Smith and M. P. Kennett, Disorder effects on superconducting tendencies in the checkerboard Hubbard model, Phys. Rev. B **88**, 214518 (2013).

[31] T. Ying, R. Mondaini, X. D. Sun, T. Paiva, R. M. Fye, and R. T. Scalettar, Determinant quantum Monte Carlo study of d-wave pairing in the plaquette Hubbard Hamiltonian, Phys. Rev. B **90**, 075121 (2014).

[32] G. Wachtel, S. Baruch, and D. Orgad, Optimal inhomogeneity for pairing in Hubbard systems with next-nearest-neighbor hopping, Phys. Rev. B **96**, 064527 (2017).

[33] G. Mazza, A. Amaricci, and M. Capone, Interface and bulk superconductivity in superconducting heterostructures with enhanced critical temperatures, Phys. Rev. B **103**, 094514 (2021).

[34] M. Danilov, E. G. C. P. van Loon, S. Brener, S. Iskakov, M. I. Katsnelson, and A. I. Lichtenstein, Degenerate plaquette physics as key ingredient of high-temperature superconductivity in cuprates, npj Quantum Mater. **7**, 50 (2022).

[35] S. A. Kivelson, I. P. Bindloss, E. Fradkin, V. Oganesyan, J. Tranquada, A. Kapitulnik, and C. Howald, How to detect fluctuating stripes in the high-temperature superconductors, Rev. Mod. Phys. **75**, 1201 (2003).

[36] E. Berg, E. Fradkin, S. A. Kivelson, and J. M. Tranquada, Striped superconductors: how spin, charge and superconducting orders intertwine in the cuprates, New J. Phys. **11**, 115004 (2009).

[37] M. Vojta, Lattice symmetry breaking in cuprate superconductors: stripes, nematics, and superconductivity, Adv. Phys. **58**, 699 (2009).

[38] E. W. Huang, C. B. Mendl, H.-C. Jiang, B. Moritz, and T. P. Devereaux, Stripe order from the perspective of the Hubbard model, npj Quantum Mater. **3**, 22 (2018).

[39] D. F. Agterberg, J. S. Davis, S. D. Edkins, E. Fradkin, D. J. Van Harlingen, S. A. Kivelson, P. A. Lee, L. Radzihovsky, J. M. Tranquada, and Y. Wang, The physics of pair-density waves: cuprate superconductors and beyond, Annu. Rev. Condens. Matter Phys. **11**, 231 (2020).

[40] J. M. Tranquada, Cuprate superconductors as viewed through a striped lens, Adv. Phys. **69**, 437 (2020).

[41] J. P. Dehollain, U. Mukhopadhyay, V. P. Michal, Y. Wang, B. Wunsch, C. Reichl, W. Wegscheider, M. S. Rudner, E. Demler, and L. M. K. Vandersypen, Nagaoka ferromagnetism observed in a quantum dot plaquette, Nature (London) **579**, 528 (2020).

[42] S. R. Manmana, A. Muramatsu, and R. M. Noack, Time evolution of one-dimensional quantum many body systems, in

Lectures on the Physics of Highly Correlated Electron Systems IX: Ninth Training Course in the Physics of Correlated Electron Systems and High-T_c Superconductors, AIP Conference Proceedings Vol. 789 (American Institute of Physics, College Park, MD, 2005), p. 269.

[43] P. Prelovšek and J. Bonča, Ground state and finite temperature Lanczos methods, in *Strongly Correlated Systems: Numerical Methods*, edited by A. Avella and F. Mancini (Springer, Berlin, 2013), pp. 1–30.

[44] F. Maislinger and H. G. Evertz, Impact ionization and multiple photon absorption in the two-dimensional photoexcited Hubbard model, Phys. Rev. B **105**, 045114 (2022).

[45] B.-X. Zheng, C.-M. Chung, P. Corboz, G. Ehlers, M.-P. Qin, R. M. Noack, H. Shi, S. R. White, S. Zhang, and G. K.-L. Chan, Stripe order in the underdoped region of the two-dimensional Hubbard model, Science **358**, 1155 (2017).

[46] E. W. Huang, C. B. Mendl, S. Liu, S. Johnston, H.-C. Jiang, B. Moritz, and T. P. Devereaux, Numerical evidence of fluctuating stripes in the normal state of high-T_c cuprate superconductors, Science **358**, 1161 (2017).

[47] B. Ponsioen, S. S. Chung, and P. Corboz, Period 4 stripe in the extended two-dimensional Hubbard model, Phys. Rev. B **100**, 195141 (2019).

[48] L. D'Alessio and M. Rigol, Long-time Behavior of Isolated Periodically Driven Interacting Lattice Systems, Phys. Rev. X **4**, 041048 (2014).

[49] S. Sorg, L. Vidmar, L. Pollet, and F. Heidrich-Meisner, Relaxation and thermalization in the one-dimensional Bose-Hubbard model: A case study for the interaction quantum quench from the atomic limit, Phys. Rev. A **90**, 033606 (2014).

[50] A. Bauer, F. Dorfner, and F. Heidrich-Meisner, Temporal decay of Néel order in the one-dimensional Fermi-Hubbard model, Phys. Rev. A **91**, 053628 (2015).

[51] T. A. Maier, M. Jarrell, T. C. Schulthess, P. R. C. Kent, and J. B. White, Systematic Study of d-Wave Superconductivity in the 2D Repulsive Hubbard Model, Phys. Rev. Lett. **95**, 237001 (2005).

[52] M. Först, R. I. Tobey, H. Bromberger, S. B. Wilkins, V. Khanna, A. D. Caviglia, Y.-D. Chuang, W. S. Lee, W. F. Schlotter, J. J. Turner, M. P. Minitti, O. Krupin, Z. J. Xu, J. S. Wen, G. D. Gu, S. S. Dhesi, A. Cavalleri, and J. P. Hill, Melting of Charge Stripes in Vibrationally Driven La$_{1.875}$Ba$_{0.125}$CuO$_4$: Assessing the Respective Roles of Electronic and Lattice Order in Frustrated Superconductors, Phys. Rev. Lett. **112**, 157002 (2014).

[53] Y. Wang, Y. Chen, T. P. Devereaux, B. Moritz, and M. Mitrano, X-ray scattering from light-driven spin fluctuations in a doped Mott insulator, Commun. Phys. **4**, 212 (2021).

[54] X. Chen, Z.-C. Gu, and X.-G. Wen, Local unitary transformation, long-range quantum entanglement, wave function renormalization, and topological order, Phys. Rev. B **82**, 155138 (2010).